

RESEARCH ARTICLE

Cytoplasmic dynein pushes the cytoskeletal meshwork forward during axonal elongation

Douglas H. Roossien¹, Phillip Lamoureux² and Kyle E. Miller^{2,*}

ABSTRACT

During development, neurons send out axonal processes that can reach lengths hundreds of times longer than the diameter of their cell bodies. Recent studies indicate that *en masse* microtubule translocation is a significant mechanism underlying axonal elongation, but how cellular forces drive this process is unknown. Cytoplasmic dynein generates forces on microtubules in axons to power their movement through ‘stop-and-go’ transport, but whether these forces influence the bulk translocation of long microtubules embedded in the cytoskeletal meshwork has not been tested. Here, we use both function-blocking antibodies targeted to the dynein intermediate chain and the pharmacological dynein inhibitor ciliobrevin D to ask whether dynein forces contribute to *en bloc* cytoskeleton translocation. By tracking docked mitochondria as fiducial markers for bulk cytoskeleton movements, we find that translocation is reduced after dynein disruption. We then directly measure net force generation after dynein disruption and find a dramatic increase in axonal tension. Taken together, these data indicate that dynein generates forces that push the cytoskeletal meshwork forward *en masse* during axonal elongation.

KEY WORDS: Axonal elongation, Dynein, Neuronal biophysics

INTRODUCTION

Axonal elongation is the process by which neurons send out long cellular projections that will eventually form synapses with prescribed targets. Proper extension and navigation through a complex tissue is guided by extracellular signaling molecules, many of which converge on the cytoskeleton (Dickson, 2002). By convention, the axonal cytoskeleton was considered to be stationary during elongation and it was thought that the new axon was formed by the addition of new material at the growth cone, either through cytoskeleton polymerization or the deposition of material by motor-driven transport (Goldberg and Burmeister, 1986; Dent and Gertler, 2003; Lowery and Van Vactor, 2009). Recently, however, there have been several studies of bulk translocation in multiple model systems, such as *Aplysia* growth cones (Lee and Suter, 2008), cultured chick sensory neurons (Miller and Sheetz, 2006; Lamoureux et al., 2010a) and *Drosophila* motoneurons *in vivo* (Roossien et al., 2013). They indicate that the classic findings of bulk microtubule translocation in *Xenopus* neurons (Reinsch et al., 1991; Chang et al., 1998)

were not a species-specific phenomenon, but rather a broadly conserved mechanism for elongation. From this, a new model for axonal elongation has emerged, termed ‘stretch and intercalation’ (SAI) (Suter and Miller, 2011), in which forces cause the microtubule-rich central domain (C-domain) of the growth cone to advance in bulk. This is paired with stretching of the axon, which is followed by intercalated mass addition along the axon to prevent thinning (Lamoureux et al., 2010). In terms of the cytoskeleton, stretching presumably occurs because filaments are sliding apart either through pulling or pushing forces generated by molecular motors (Suter and Miller, 2011; Lu et al., 2013; Roossien et al., 2013). It is worth noting that because adhesions along the axon dissipate forces generated in the growth cone (O’Toole et al., 2008), these *en masse* movements of the cytoskeleton occur only in the distal axon, whereas the cytoskeletal framework is stationary near the cell body (Lim et al., 1990; Okabe and Hirokawa, 1990).

To track *en masse* movement of the cytoskeletal meshwork, we monitor the movement of mitochondria docked to cytoskeletal elements. Mitochondria are large organelles that can be easily visualized under low-light conditions using fluorescent dyes. After motor-driven fast transport (Pilling et al., 2006) at a rate of ~3600 $\mu\text{m}/\text{h}$, mitochondria stably dock to microtubules through syntrophin (Hirokawa, 1982; Kang et al., 2008) to actin filaments (Pathak et al., 2010) and intermediate or neuronal filaments (Hirokawa, 1982; Wagner et al., 2003). Docking occurs at regular intervals along the axon (Miller and Sheetz, 2004), where mitochondria can remain in position for several hours at a time (Morris and Hollenbeck, 1993; Chada and Hollenbeck, 2004; Miller and Sheetz, 2004; Saxton and Hollenbeck, 2012). Along the length of the axon, docked mitochondria slowly move forward at a rate of 1–50 $\mu\text{m}/\text{h}$, with a velocity profile that increases along the length of the axon (O’Toole et al., 2008). In previous studies, we have shown that this is paired with the forward advance of beads bound to the outside of the axon and axonal branch points (Lamoureux et al., 2010a), which together indicates that this slow movement reflects the bulk movement or stretching of the underlying cytoskeletal meshwork. Because this movement occurs at a rate of ~1000 times slower than fast transport, it is straightforward to distinguish between this ‘low velocity transport’ and fast axonal transport in kymographs (Miller and Sheetz, 2006). Using this approach, we have shown that axonal stretching occurs during axonal elongation *in vivo* (Roossien et al., 2013), in cultured neurons from various species (Miller and Sheetz, 2006; O’Toole et al., 2008; Lamoureux et al., 2010a; Lamoureux et al., 2010b; Roossien et al., 2013) and in response to forces generated in or applied to the growth cone (O’Toole et al., 2008; Lamoureux et al., 2010a). Furthermore, in the field of non-neuronal cell biophysics, docked mitochondria are well-accepted fiducial markers for bulk subcellular deformation (Wang et al., 2001; Knight et al., 2006; Gilchrist et al., 2007; Wang et al.,

¹Cell and Molecular Biology Program, Michigan State University, 288 Farm Ln Room 336, East Lansing, MI 48824, USA. ²Department of Zoology, Michigan State University, 288 Farm Ln Room 336, East Lansing, MI 48824, USA.

*Author for correspondence (kmiller@msu.edu)

2007; del Alamo et al., 2008; Bell et al., 2012; Silberberg and Pelling, 2013).

The question of what powers bulk translocation of the cytoskeletal meshwork has not been answered, but microtubule-based motors, such as cytoplasmic dynein, are logical candidates. Dynein is essential for the proper growth and maintenance of the axon. Identified roles for dynein in growing axons include driving retrograde transport of membrane organelles (Schnapp and Reese, 1989) and establishment of the initial microtubule bundle during axon initiation (Ahmad et al., 1998; Dehmelt et al., 2006). Dynein forces in the growth cone are thought to be required for microtubules to resist retrograde actin flow (Myers et al., 2006; Vallee et al., 2009) and, along the axon, they resist actomyosin-based retraction and power ‘stop-and-go’ transport of individual short microtubules (Ahmad et al., 1998; He et al., 2005; Ahmad et al., 2006). Previous studies of dynein function in axons have reported a decrease in elongation following dynein disruption (Ahmad et al., 2000; Ahmad et al., 2006; Myers et al., 2006; Grabham et al., 2007), but whether dynein contributes to *en masse* cytoskeleton movement is unknown.

Here, we used function-blocking dynein-specific antibodies and acute pharmacological disruption with the recently published dynein inhibitor ciliobrevin D (CiLD) to study the role of dynein in axonal elongation. We found that both treatments resulted in a decrease in axonal elongation. By using docked mitochondria as fiducial markers of the axonal cytoskeletal meshwork before and after dynein disruption, we also found that dynein activity drives the forward translocation of the cytoskeletal meshwork during elongation. To determine whether dynein contributes to axonal elongation by pulling or pushing material forward, we measured net force generation in axons and then added CiLD to disrupt dynein. In response, we found an increase in neuronal tension. Taken together, these studies indicate that dynein pushes microtubules embedded in the cytoskeletal meshwork forward in bulk during axonal elongation.

RESULTS

Disruption of dynein activity reduces axonal elongation by causing bulk retraction of the cytoskeletal meshwork

The microinjection of function-blocking antibodies targeted against the N-terminal 63 amino acids of the 74-kDa dynein intermediate chain (α DIC) has become a gold standard for perturbing dynein function. In non-neuronal cells, it has been used to study the positioning of the microtubule-organizing centre (MTOC) (Palazzo et al., 2001), directed cell migration (Dujardin et al., 2003), and spindle formation and positioning during mitosis (Faulkner et al., 2000; O’Connell and Wang, 2000). In neurons, α DIC has been used to probe dynein function in retrograde axonal transport in rat hippocampal neurons (Yi et al., 2011) and in laminin-induced neurite elongation of chick sensory neurons (Grabham et al., 2007). We therefore sought to disrupt dynein function through the microinjection of α DIC in elongating axons grown under our culture conditions (i.e. neurons grown on plastic dishes coated with poly-ornithine).

In our experiments, both α DIC and control antibodies (nonspecific mouse IgG proteins) were mixed at 10 mg/ml with 0.1 μ g/ml FITC–dextran, allowing for visualization of fluid flow and screening for injected neurons. Injections were carried out in neuronal cell bodies at ~18–20 h after plating. After 2 h, neurons were screened for successful injection based on the presence of the fluorescent marker and morphologically normal rounded cell bodies (Fig. 1A). As a positive control to verify that injected

α DIC antibodies decrease dynein function, we analyzed dynein-dependent fast mitochondrial transport (Saxton and Hollenbeck, 2012; Pilling et al., 2006). Mitochondria were labeled with MitoTracker immediately following microinjection and were allowed to recover for 2 h. Flux was then measured by counting the number of mitochondria that passed the midway point in the axon. We found no significant difference in fast mitochondrial flux in the retrograde direction between non-injected neurons and those injected with control IgG (Fig. 1B). Axons injected with α DIC, by contrast, had average retrograde flux of 1.15 ± 1.39 mito/h [mean \pm 95% confidence intervals (CI)], significantly lower than both non-injected axons and those injected with IgG (Fig. 1B; 5.60 ± 1.87 and 8.31 ± 2.11 , respectively). This is in agreement with a previous analysis of retrograde axonal transport of other membrane organelles after α DIC injection (Yi et al., 2011). We also found, as reported previously (Yi et al., 2011), that fast anterograde flux was reduced in neurons injected with IgG. When we compared anterograde flux in IgG-injected neurons with that of α DIC-injected neurons, we found a further significant decrease (Fig. 1B). Although this might seem surprising, it has also been reported in other systems where dynein was disrupted (Martin et al., 1999). Taken together, these experiments verify that the microinjection of α DIC significantly reduces dynein activity.

We have previously shown that neurons grow by axonal stretching and bulk forward movement of the cytoskeletal meshwork (Miller and Sheetz, 2006; O’Toole et al., 2008; Lamoureux et al., 2010a; Lamoureux et al., 2010b; Roossien et al., 2013). To test whether dynein contributes to this process, we tracked the movement of docked mitochondria (Morris and Hollenbeck, 1993; Saxton and Hollenbeck, 2012) after microinjection of IgG and α DIC antibodies into chick sensory neurons. Fig. 1C shows an axon from a control neuron injected with IgG. To show the different populations of mitochondria moving by fast retrograde transport, fast anterograde transport and bulk transport, the kymograph has been duplicated and color-coded arrows have been added (Fig. 1E). We found that in growth cones from neurons injected with IgG controls, docked mitochondria in the growth cone advanced in tandem with the growth cone (Fig. 1C). This suggests that the growth cone advances in bulk as one coherent unit. In addition, docked mitochondria in the distal axon advanced during elongation. From this we infer that the cytoskeletal meshwork is advancing *en masse*. By contrast, docked mitochondria in axons from neurons injected with α DIC exhibited slow retrograde movements, suggesting that the cytoskeletal meshwork was retracting (Fig. 1D).

To quantify movements following microinjection, mitochondrial velocities were sorted based on their initial distance from the growth cone, placed into 25- μ m bins and averaged (Fig. 1F). The velocities of docked mitochondria from IgG control axons increased as the distance from the growth cone decreased, becoming increasingly spread apart. Likewise, based on the analysis of phase images, the IgG controls grew at 24.9 ± 7.9 μ m/h (mean \pm 95% CI). This suggests, as has been reported previously (Miller and Sheetz, 2006; O’Toole et al., 2008; Lamoureux et al., 2010a; Roossien et al., 2013), that the cytoskeletal meshwork is being stretched, similar to a piece of ‘silly-putty’ with a fixed end at the cell body and a pulled end at the growth cone. By contrast, in neurons injected with α DIC, growth cones were stationary with an average velocity of -1.5 ± 3.8 μ m/h (mean \pm 95% CI; $P < 0.01$; unpaired two-tailed

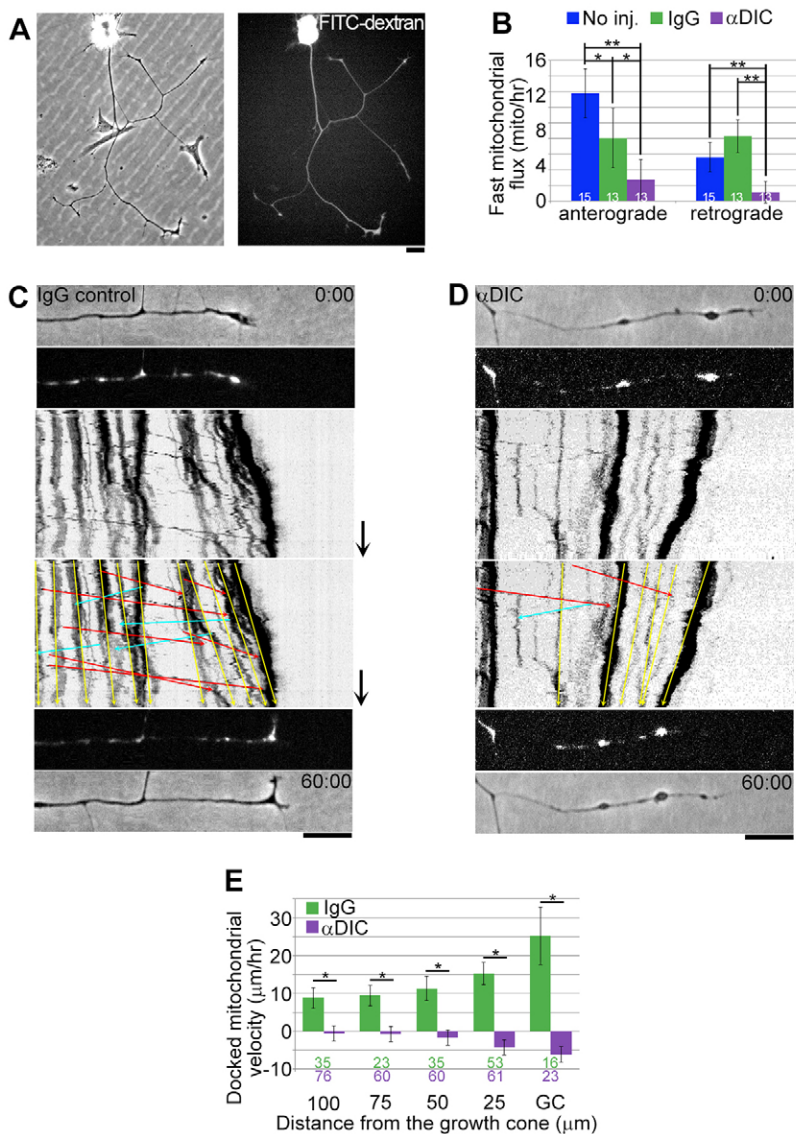


Fig. 1. Microinjection of 74.1 dynein intermediate chain antibodies reduces axonal elongation by inducing retraction of the axonal meshwork.

Neurons were microinjected with function-blocking antibodies against the dynein intermediate chain (α DIC) or nonspecific mouse IgG control antibodies mixed with FITC–dextran. (A) A neuron injected with α DIC shows normal cell body and neurite morphology at 2 h after injection. Successful injection is confirmed by the presence of FITC–dextran throughout the entire neuron. Scale bar: 25 μ m. (B) Fast mitochondrial flux in both the anterograde and retrograde direction, measured by counting the number of mitochondria that passed the mid-way point of the axon, is reduced by α DIC injection (inj.) compared with that observed following injection of IgG controls.

*significant at $\alpha=0.05$, **significant at $\alpha=0.01$ (post-hoc Tukey's test). (C) Docked mitochondria were tracked following injection with IgG control antibodies. The color-inverted kymograph shows that docked mitochondria in the distal axon and in the growth cone advance during elongation. This kymograph has been duplicated in E and labeled with color-coded arrows representing different pools of mitochondrial motion: yellow, docked mitochondria translocation; red, anterograde fast transport; blue, retrograde fast transport. Time arrows: 15 min. Scale bar: 20 μ m. (D) Corresponding image series showing that mitochondria in neurons injected with α DIC antibodies undergo bulk retrograde movement, suggesting that the cytoskeletal meshwork is retracting.

(F) Mitochondrial velocities were sorted based on their initial distance from the growth cone, binned and averaged. The distally increasing velocity gradient after IgG injection is consistent with axonal stretching. The negative velocities after α DIC injection indicate bulk retraction. GC, growth cone. All data show the mean \pm 95% CI. * $P < 0.01$ (unpaired two-tailed Student's *t*-test). Values at the bottom of the bars show the number of mitochondria used for each group.

Student's *t*-test) and docked mitochondria in the distal axon moved rearwards (Fig. 1F). These data indicate that dynein powers axonal elongation and bulk forward translocation of the cytoskeletal meshwork.

Acute disruption of dynein with the pharmacological inhibitor CiID causes retraction of the axonal cytoskeleton

Ciliobrevins are a recently discovered class of small-molecule dynein inhibitors (Firestone et al., 2012). They compete with ATP at its binding site in the dynein motor, thus increasing the time that dynein spends attached to the microtubule in the post-power-stroke conformation (Kikkawa, 2013). The use of these inhibitors offers advantages over previous approaches (i.e. RNA interference, microinjection and genetic knockout) in that they can be acutely and systematically applied. Of these inhibitors, the D form of ciliobrevin (CiID) was shown to most effectively reduce dynein function as measured in microtubule gliding and vesicular transport assays (Firestone et al., 2012). Our first step in using CiID was to find a concentration that blocked elongation to an extent similar to that seen following microinjection of α DIC. We found that at 60 μ M elongation began to slow, at 100 μ M

growth cones became stationary, and at 150 μ M and above retraction occurred (Fig. 2A). To verify the disruption of dynein function by CiID, we measured fast mitochondrial transport as discussed above at CiID concentrations of 60 and 100 μ M, and we found effects similar to those seen with microinjection of α DIC. Retrograde transport was reduced to 66% and 22% of that observed in DMSO controls at 60 and 100 μ M CiID, respectively (Fig. 2B). Anterograde flux was not affected at 60 μ M, but was decreased with 100 μ M CiID (Fig. 2B). We note that previous studies using ciliobrevins reported a bidirectional disruption of transport of other membrane vesicles (Firestone et al., 2012; Lu et al., 2013). The similarity in results between 100 μ M CiID and α DIC microinjection suggests that this concentration is appropriate for impairing dynein function.

Next, we tracked the movement of docked mitochondria before and after the addition of 100 μ M CiID. In total, 32 elongating axons were imaged at 1-min intervals for 20 min prior to and 60 min after CiID addition in both phase and fluorescent channels. As seen in the phase images, CiID causes advancing growth cones to retract briefly, after which they become stationary (Fig. 2C; supplementary material Movie 1). During

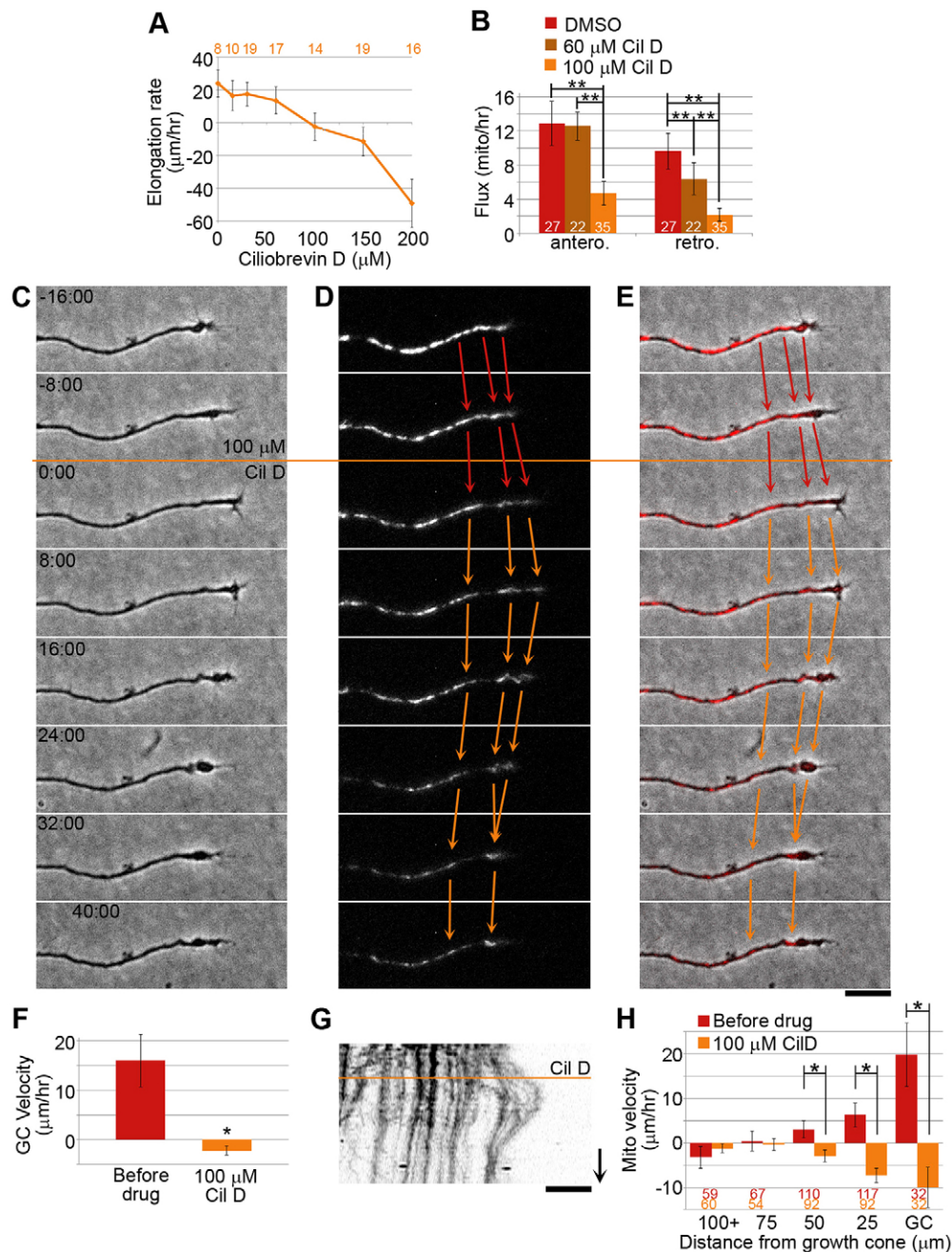


Fig. 2. Acute pharmacological disruption of dynein with CiID slows axonal elongation and induces retraction of the axonal meshwork.

(A) Disruption of dynein with CiID reduces the rate of elongation in a dose-dependent manner. Orange numbers at the top are the number of axons in each group; 0 μM is the DMSO control.

(B) Disruption of dynein reduces fast mitochondrial flux in a dose-dependent manner. Numbers in white at the base of the bars are the numbers of axons used in each group. (C) Acute disruption of dynein initially induces retraction as seen in phase images. Afterwards, the growth cones are stationary. The orange line represents $t=0:00$ for the bath application of 100 μM CiID. (D) Acute disruption of dynein induces retraction of docked mitochondria. (E) Overlaying the fluorescent and phase images

(C,D) indicates that docked mitochondria continue to move rearward, even when the growth cone is stationary. Red arrows, pre-drug; orange arrows, post-drug. (F) The rate of growth cone advance before and after the addition of 100 μM CiID. (G) The color-inverted kymograph shows the shift from axonal stretching during elongation to bulk retraction and contraction along the axon following CiID treatment. Time arrow: 15 min. Scale bars: 20 μm .

(H) Quantitative analysis demonstrates that dynein disruption induces contraction and bulk retraction. Color-coded numbers at the bottom of the graph represent the number of mitochondria in each bin, where the growth cone bin (GC) comprises the most distal mitochondrion per axon. Note the difference in rate between GC mitochondria in H and growth cone retraction in F. All quantitative data show the mean \pm 95% CI. * $P < 0.01$ (unpaired two-tailed Student's t -test); **significant at $\alpha < 0.01$ (post-hoc Tukey's test).

the retraction phases, the distal axon retracts in an accordion-like fashion. Fig. 2D shows fluorescently labeled docked mitochondria over time. These mitochondria are moving forward as the axon elongates (red arrows), as seen in IgG-injected control neurons (Fig. 1C,E). In addition, mitochondria in the growth cone advance in tandem with the growth cone. Upon addition of 100 μM CiID, however, distal mitochondria begin retracting towards the cell body (orange arrows) (supplementary material Movie 1). This can also be seen in the mitochondrial kymograph in Fig. 2G. Overlaying the fluorescent and phase-image series shows that mitochondria in the growth cone move backward out of the growth cone when dynein is acutely disrupted (Fig. 2E). To control for the possibility that our fluorescent imaging conditions were causing retraction or impairing drug function, we measured the elongation rate of

these individual growth cones in phase images before and after CiID addition. We found that 100 μM CiID significantly decreased the rate of elongation from $16.1 \pm 5.4 \mu\text{m/h}$ to $2.8 \pm 0.9 \mu\text{m/h}$ (Fig. 2F; mean \pm 95% CI; $P < 0.01$; paired two-tailed Student's t -test). This is in agreement with the data shown in Fig. 2A, suggesting that our imaging conditions were not causing retraction or impairing drug function. To quantify mitochondrial motion, velocities were measured before and after CiID treatment, sorted based on their distance from the growth cone, placed in 25 μm bins and averaged (Fig. 2H). Before CiID addition, mitochondria were stationary in the proximal axon and moved forward in the distal axon (Fig. 2H). Treatment with CiID caused a rapid and significant change from bulk forward advance of the cytoskeletal meshwork in the distal axon (red bars, before drug) to retraction (orange bars, 100 μM

CiID). This suggests that the accordion-like compaction is due to the cytoskeletal meshwork being pulled backward in bulk. These data are consistent with those found after dynein disruption with α DIC and, taken together, suggest that dynein powers bulk forward movement of the axonal cytoskeleton and growth cone during axonal elongation.

Local disruption of dynein in the growth cone and distal axon causes retraction independently of fast axonal transport

In prior studies investigating the role of kinesin and dynein in axonal elongation, a caveat has been that it is difficult to separate their activity in the growth cone from their role in delivering new material to the distal axon. To this end, we focally applied CiID to the growth cone and distal 30 μm of the axon for 20 min using micropipettes in a flow chamber. In Fig. 3A, an image series over a 20-min period shows the local application of 150 μM CiID as a

red overlay on the phase images in the left column (see supplementary material Movie 2). We used this concentration to ensure a robust growth cone response and to account for rapid diffusion. Fig. 3A shows the growth cone advancing during the 20-min period of pre-treatment observation, then retracting during direct CiID application at the growth cone. To address potential toxic or off-target effects of high concentrations of CiID, washout experiments were performed by monitoring axons after the removal of the micropipette (Fig. 3B). We found that, after washout, normal morphology and behavior was restored, and the growth cones resumed forward advance, suggesting that CiID does not cause retraction by damaging the growth cone and distal axon. Control growth cones treated with DMSO, by contrast, continued to advance during fluid application (Fig. 3C). We tracked the position of individual growth cones at 1-min intervals and normalized them by adjusting the initial position to 0 μm .

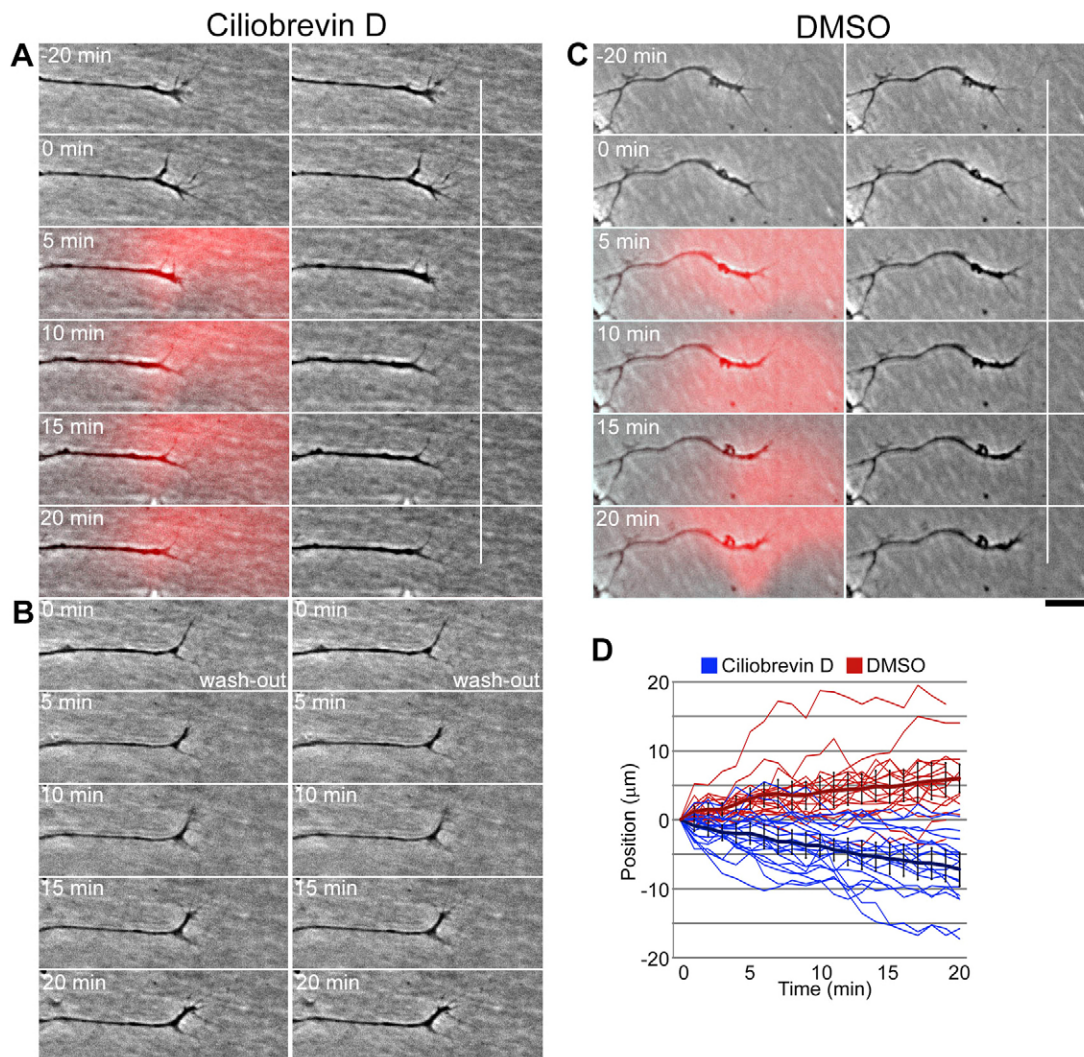


Fig. 3. Focal disruption of dynein in the growth cone and distal axon causes axonal retraction. (A) Focal application of CiID, to disrupt dynein in the growth cone and distal axon, induced axonal retraction. The extent of drug application is shown by the red overlay in the phase images. (B) Growth cones treated with CiID were tracked after removal of the micropipette in a washout experiment. They resumed normal morphology and forward elongation. (C) Focal application of DMSO, as a control, had no effect on axonal elongation. Scale bar: 20 μm . (D) Individual growth cone movements were normalized for initial position and plotted during the 20-min treatment with CiID (blue) or DMSO (red). Thick dark bars show the mean growth cone position at each 1-min interval. Control growth cones grew at rate of 17.4 ± 7.0 $\mu\text{m}/\text{h}$ (mean \pm 95% CI). Focal disruption of dynein induced retraction at an average rate of -22.1 ± 6.9 $\mu\text{m}/\text{h}$ (mean \pm 95% CI). Growth cones treated with CiID resumed growth at 13.6 ± 3.2 $\mu\text{m}/\text{h}$ during washout. Error bars show 95% CI.

When plotted together, DMSO-treated growth cones continued to advance, whereas those treated with CiID retracted (Fig. 3D). The thick dark lines on the graph in Fig. 3D represent the average position at each time-point, showing that dynein disruption in the growth cone and distal axon is sufficient for growth cone retraction. We calculated the average growth cone velocity based on the final change in position at the end of the experiment and found it to be $17.4 \pm 7.0 \mu\text{m/h}$ (mean \pm 95% CI; $n=18$) in control growth cones and $-22.1 \pm 6.9 \mu\text{m/h}$ ($n=20$; $P<0.01$) in CiID-treated growth cones. After washout, the CiID-treated growth cones resumed elongating at an average rate of $13.6 \pm 5.6 \mu\text{m/h}$ (mean \pm 95% CI; supplementary material Movie 2). These data suggest that dynein functions to drive axonal elongation in the distal portion of the axon independently of its activity in the proximal axon.

Ciliobrevin D decreases translocation in the absence of non-muscle myosin II activity

Dynein activity is required to resist non-muscle myosin II (NMII)-induced growth cone retraction (Ahmad et al., 2000), but whether these two motors cooperate in bulk translocation of the cytoskeleton is unknown. We therefore combined CiID treatment with NMII disruption using blebbistatin (Straight et al., 2003). In these experiments, mitochondria were tracked in 28 axons for 15 min prior to drug addition (Fig. 4, blue arrows and bars), for 45 min during treatment with 50 μM blebbistatin (Fig. 4, yellow arrows and bars) and then for a final 45 min in the presence of both blebbistatin and 100 μM CiID (Fig. 4, orange arrows and bars). We found that NMII disruption caused an increase in bulk translocation of the growth cone from 21.9 ± 7.4 to $31.2 \pm 5.2 \mu\text{m/h}$ (mean \pm 95% CI; Fig. 4). Subsequent inhibition of dynein resulted in a reduction in elongation to $13.1 \pm 3.2 \mu\text{m/h}$. This is significantly lower in the presence of CiID compared with either pre-treatment or 50 μM blebbistatin alone ($\alpha=0.01$, post-hoc Tukey's test). In addition, mitochondrial velocities along the length of the axon in the combined presence of CiID and blebbistatin were significantly lower than pre-treatment velocities. Of particular interest, we note that neurons still grew and material along the axon moved forward when dynein and NMII were simultaneously disrupted; in contrast to disruption of dynein alone (compare Fig. 1E and Fig. 2H). Taken together, these experiments suggest that NMII generates forces that oppose the bulk advance of the growth cone and that there are other motors, besides dynein, that power forward translocation of the axonal meshwork.

Dynein disruption causes an increase in axonal tension

There are two broad explanations for how dynein could be powering the forward translocation of the cytoskeletal meshwork. It could be primarily pulling microtubules forward, as seen in non-neuronal cells during spindle pole positioning (Carminati and Stearns, 1997) and migration (Dujardin et al., 2003); in which case, the disruption of dynein would be predicted to decrease net tension in the axon. Alternatively, dynein could be pushing microtubules as observed in stop-and-go transport (He et al., 2005; Ahmad et al., 2006) and in the transport of short microtubules at the cell cortex of non-neuronal cells (Mazel et al., 2014). In this case, the prediction is that the disruption of dynein will increase tension. To test this, we used force-calibrated substrate-coated towing needles in a rest-tension assay to measure changes in net axonal force generation before and after the addition of 100 μM CiID. This assay measures net forces being

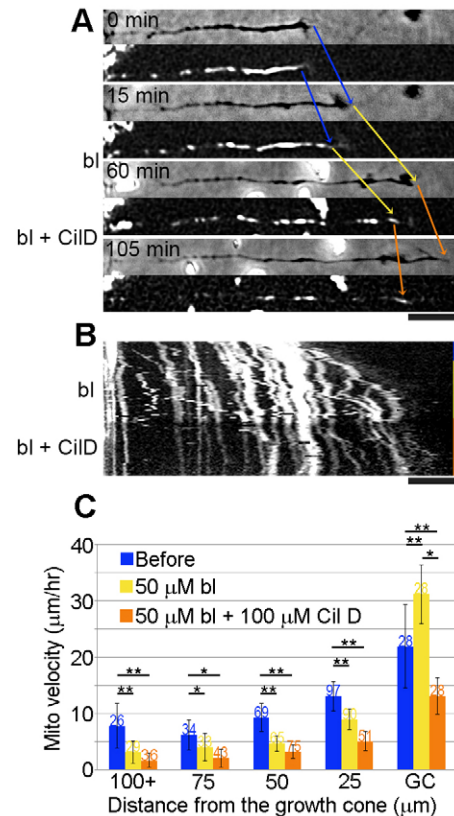


Fig. 4. An antagonistic relationship between myosin II and dynein controls bulk growth cone advance. (A) Neurons were allowed to grow for 15 min, then treated with 50 μM blebbistatin (bl) to disrupt myosin II function for 45 min, after which 100 μM CiID was added. Paired phase and fluorescent images of mitochondria show that blebbistatin increases growth cone advance (compare blue arrows to yellow arrows), whereas subsequent CiID addition reduces it (orange arrows versus yellow arrows). (B) Kymograph of docked mitochondria in the axon shown in A. Blue bar, pre-drug; yellow bar, blebbistatin; orange bar, blebbistatin+CiID. Scale bars: 20 μm . (C) Quantitative analysis of docked mitochondria illustrates that blebbistatin causes an increase in bulk growth cone translocation and a decrease along the axon. Addition of CiID causes a subsequent reduction at all points in the axon compared with pre-treatment levels. Numbers above each bar represent the number of mitochondria in each bin. GC, the most distal mitochondria in each growth cone. Data show the mean \pm 95% CI; *significant at $\alpha=0.05$, **significant at $\alpha=0.01$ (post-hoc Tukey's test).

generated in the neuron, which result from the combined activity of cytoskeletal motors, cytoskeleton dynamics and membrane tension. Furthermore, the measured forces reflect those generated in both the growth cone and along the axon. An individual force profile is shown in Fig. 5A. In red are the initial force measurements before CiID addition at 0 min, after which the measurements are plotted in blue. The arrows on the graph indicate the timespan represented by a series of phase images in Fig. 5B. When CiID is added, the growth cone pulls harder on the towing needle, as indicated by the increase in axonal tension (Fig. 5A,B; supplementary material Movie 3). Each of the 17 axons assayed responded in the same way. Force measurements for each axon were averaged over a 30-min period before CiID addition and a 30-min period after a new steady-state tension was established. On average, tension increased from 37.6 ± 10.7 to $79.8 \pm 10.9 \mu\text{dyne}$ (Fig. 5C; mean \pm 95% CI; $P<0.01$; pairwise two-tailed t -test).

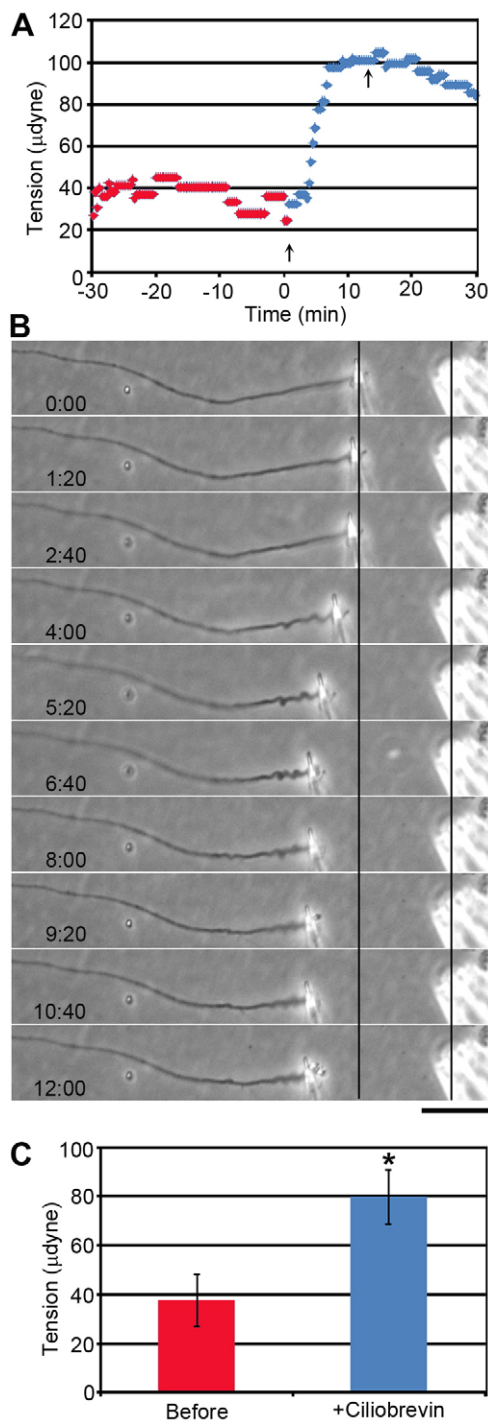


Fig. 5. Dynein disruption with CilD increases axonal tension. Force-calibrated towing needles attached to growth cones are used to measure changes in forces after dynein disruption. (A) An individual force profile shows that tension increases when 100 μM CilD is added at $t=0$ min. Red, force measurements taken before CilD; blue, force measurements taken after CilD addition. Note the steady-state force balance before and after drug addition, which was used to calculate the average tension for each axon. Arrows represent the time-span presented in B. (B) The increase in tension is seen as pulling on the needle in a series of phase images, corresponding to the time demarcated by arrows in A. $t=0:00$ represents the time of CilD addition. Vertical lines have been added to the series to show the initial position of the two needles at the time of CilD addition. Scale bar: 25 μm . (C) The average tension measurements before and after CilD addition. Data show the mean \pm 95% CI. * $P < 0.01$ (paired two-tailed Student's t -test).

DISCUSSION

In this paper, we sought to identify the molecular mechanism underlying bulk translocation of the cytoskeletal meshwork during axonal elongation (Reinsch et al., 1991; Miller and Sheetz, 2006; Lee and Suter, 2008; O'Toole et al., 2008; Schaefer et al., 2008; Lamoureux et al., 2010a; Lamoureux et al., 2010b; Roossien et al., 2013). We disrupted dynein and found a decrease in elongation, as reported previously (Ahmad et al., 2000; Ahmad et al., 2006; Myers et al., 2006; Grabham et al., 2007). By tracking the movement of docked mitochondria as fiducial markers of the cytoskeletal meshwork, we report the novel finding that dynein disruption slows elongation by reducing forward translocation of the meshwork (Figs 1, 2). Using biophysical analysis, we find that this is coupled with an increase in neuronal tension (Fig. 5). These observations indicate that dynein drives axonal elongation by generating forces that oppose contractile force generation and thus push the cytoskeletal meshwork forward *en masse*.

A major challenge in studying the role of kinesin and dynein in axonal elongation is that both are required for fast axonal transport. In particular, disruption of dynein inhibits kinesin. Furthermore, well-established approaches for disrupting dynein (i.e. RNAi and antibody microinjection) do so globally and chronically. This makes it difficult to sort the role of local dynein action at the growth cone from the long-term contribution of cargo delivery from the cell body to the growth cone. Our method here of focally applying CilD to the growth cone to disrupt dynein offers two distinct advantages; it is acute and local. Here, we show that this method also blocks axonal elongation (Fig. 3). This indicates that dynein in the growth cone and distal axon has an important role for elongation independent of that in cargo transport from the cell body.

The idea that NMII and dynein have an antagonistic relationship in elongation is well accepted. Although this has been examined in the context of stop-and-go microtubule transport (Ahmad et al., 2000; Baas and Ahmad, 2001), the role of NMII in bulk transport is unknown. To test whether NMII modulates bulk transport, we treated neurons with blebbistatin and found that bulk growth cone translocation increased (Fig. 4). Subsequent disruption of both NMII and dynein decreased elongation and bulk transport, although not nearly as much as was observed during the disruption of dynein alone. This indicates that the net function of NMII in neurons is to inhibit bulk advance of the growth cone that counters the forward translocation driven by dynein. Interestingly, bulk transport and elongation continued when both dynein and NMII were disrupted. To us, this suggests that there are additional motors contributing to this process. Based on its ability to move long microtubules into the axon during axon initiation, kinesin-1 is an exciting possibility (Lu et al., 2013) for contributing to bulk transport during axonal elongation.

To understand the biophysical contribution that dynein makes to elongation, we measured net axonal forces after treatment with CilD. We found that disruption of dynein increased the force with which the growth cone pulled the towing needle rearwards (Fig. 5). Thus, dynein disruption both increases neuronal tension and induces retraction of the growth cone. Based on our experiments using the NMII inhibitor blebbistatin, we think that the simplest explanation is that NMII normally generates contractile forces that oppose elongation, whereas dynein generates counteracting pushing forces to assist growth cone advance. Speculative subcellular mechanisms to explain how

dynein might be generating forces that contribute to bulk transport are outlined in Fig. 6. These include the possibilities that dynein targeted to actin at the cell cortex either by IQGAP1 (Fukata et al., 2002) or Num1 (Markus et al., 2009) slides microtubules forward (Pavin and Tolić-Norrelykke, 2013). Dynein bound to the plus-ends of microtubules through LIS1 (also known as PAFAH1B1) and CLIP-170 (also known as CLIP1) drives microtubule telescoping (Vaughan et al., 1999; Kholmanskikh et al., 2006). Alternatively, dynein bound to the plasma membrane independently of cortical actin captures the plus ends of microtubules and moves them forward (Kozłowski et al., 2007; Gusnowski and Srayko, 2011). By contrast, NMII could inhibit elongation by acting as a barrier to the forward advance of microtubules in the growth cone (Schaefer et al., 2002; Hur et al., 2011; Stiess and Bradke, 2011) and/or by generating contractile forces in the axon that oppose telescoping of microtubules (Joshi et al., 1985; Ahmad et al., 2000; Gallo, 2004; Bernal et al., 2007). An important future challenge will be to integrate these different force-generating mechanisms (some of which appear to pull and others that appear to push) into a coherent model for axonal elongation.

It is recognized that dynein is important for cell migration and axonal elongation. Great progress has been made in understanding the molecular basis of dynein regulation in these

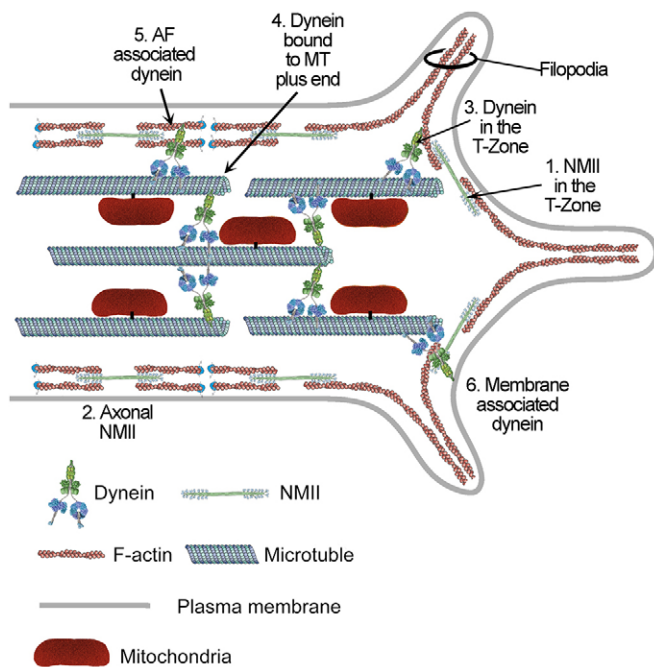


Fig. 6. Subcellular model for dynein and NMII motor function in the axon and growth cone. This model proposes the following intracellular interactions between actin, NMII, microtubules and dynein: (1) NMII in the T-zone drives retrograde actin flow and turnover that could oppose forward translocation; (2) NMII in the cell cortex along the axon generates contractile forces that could oppose axon stretching; (3) Dynein bound to actin in the T-zone might move microtubules forward; (4) Dynein bound to two neighboring microtubules (MT) could generate forces that cause them to telescope apart; (5) Dynein might use cortical actin along the axon to slide long microtubules forward (AF, actin filament); (6) Dynein might be anchored in the plasma membrane in the growth cone or along the axon independently of cortical actin, where it could capture microtubules and move them forward. NMII and actin were modified from Lodish et al., 2000. Dynein modified from Vale, 2003. Microtubules modified from Cheeseman and Desai, 2008.

contexts. LIS1 and dynactin, for example, play important roles in dynein regulation (Dujardin et al., 2003; Lansbergen et al., 2004). Both of these interact with a number of other regulatory proteins, such as IQGAP1 and CLIP-170, which are downstream targets of Rho family signaling (Fukata et al., 2002; Watanabe et al., 2004; Gomes et al., 2005; Kholmanskikh et al., 2006). Our work suggests a novel biomechanical model (Fig. 6) that potentially provides an important new link in the chain between guidance cues, signaling pathways, dynein regulation and growth cone motility.

MATERIALS AND METHODS

Cell culture

Neurons from chick dorsal root ganglia were isolated and cultured as described previously in L-15 medium supplemented with 0.6% glucose, 1 mM glutamine, 100 U/ml penicillin, 100 µg/ml streptomycin sulfate, 10% fetal calf serum, 25 ng/ml 7S nerve growth factor (Harlan Bioproducts, Indianapolis, IN) and N9 growth supplement (Lamoureux et al., 2010a). Polystyrene culture dishes (Corning; Tewksbury, MA) were treated with 0.01% poly-ornithine for 30 min then rinsed three times with sterile dH₂O.

Drug treatments

Stock (–)-blebbistatin (Sigma; St Louis, MO) was made up to 50 mM in DMSO. Prior to its addition to the culture dish, stock blebbistatin was pre-warmed and diluted 660-fold in supplemented L-15 medium, sonicated for 5 min, then incubated at 37°C for at least 30 min. Final dilutions of 1:6 were performed directly into the culture dish during image acquisition, giving a final blebbistatin concentration of 50 µM. The ciliobrevin D (Millipore; Billerica, MA) stock solution was made up to 60 mM in DMSO. The handling of CilD was identical to that of blebbistatin, with final dilutions always at 1:6 for all concentrations used. For focal application, CilD was diluted to 150 µM in PBS containing 1 mg/ml Texas-Red-dextran (10 kDa) (Invitrogen; Carlsbad, CA), sonicated for 10 min, then stored at 37°C until use. Solutions were back-loaded into TW100F-4 glass micropipettes (World Precision Instruments; Sarasota, FL) pulled on a Sutter Instruments P-97 Flaming/Brown puller. To maximize focal application at the growth cone, the micropipette tips were positioned within 10–20 µm of the growth cone within a 10-ml flow chamber set to a flow rate of 0.42 ml/min. This resulted in drug application that was highest at the growth cone and tapered away over the adjoining 20–30 µm of the axon. Pressure was manually applied to the micropipette using a 10 ml syringe connected through rubber tubing. Manual pressure, in combination with monitoring the fluid as it comes out of the pipette by fluorescence, was used instead of a Picospritzer because it allows for tighter control of fluid flow out of the pipette. Phase images were captured every 10 s, and fluorescent images were captured every 1 min using 100-ms exposures.

Microinjection

Antibodies targeted to the dynein intermediate chain (74.1; Millipore; Billerica, MA) were concentrated to 10 mg/ml in sterile injection buffer (100 mM HEPES, 140 mM KCl) mixed with 1 µg/ml FITC-dextran (134 kDa) (Sigma; St Louis, MO), using Millipore Amicon Ultra 0.5-ml 50 K centricon devices (Millipore; Billerica, MA) spun at 10,000 *g* at 4°C for 10 min. The molecular weight of dextran was chosen so as to be similar to the molecular weight of IgG antibodies. Non-specific mouse IgG antibodies (Sigma; St Louis, MO) were used as control as in previous studies (Grabham et al., 2007; Yi et al., 2011), but at 10 mg/ml. Microinjection was carried out in chick sensory neuronal cultures ~18 h after plating. Antibodies were back-loaded into the same micropipettes as above. Flow was started by manually pushing ~2 cc of air into a 10-ml syringe connected to the needle holder with rubber tubing. This was sufficient to supply a steady flow of fluid for 30–45 min. After injection into neuronal cell bodies, dishes were recovered for 2 h, then successfully injected neurons were screened by the presence of fluorescent dextran in the cell and for having normally rounded cell bodies.

Mitochondrial imaging

Chick sensory neurons were labeled with 0.1 μM MitoTracker Red CMXRos (Invitrogen; Carlsbad, CA) in L-15 for 5 min at room temperature and recovered in fresh L-15 for 1 h at 37°C. For imaging, culture dishes were held in a 'ringcubator' (Heidemann et al., 2003) set to 38°C on a Leica DM IRB inverted microscope and observed with an N Plan L 40 \times /0.55 corrPh2 with an adjustable collar infinity/0-2/c objective. Cells were illuminated with a 100-W xenon lamp attenuated 98% with neutral-density filters through a TexasRed 49008 ET cube (Chroma; Rockingham, VT) for visualization of MitoTracker. Transmitted light exposure was controlled with a VMM-D3 controller and CS25 shutter (Vincent Associates; Rochester, NY). Fluorescent light exposure was controlled with a Lambda 10-C (Sutter Instruments; Novato, CA). Acquisitions were controlled using micro-manager software (US National Institutes of Health) (Edelstein et al., 2010). Exposure times for mitochondrial images were set to 100 ms, except for the combined blebbistatin and CilD treatments, which required 250-ms exposures. For fast transport imaging, fluorescent images were captured at 10-s intervals, whereas phase images were captured every 5 min. For all other mitochondrial time-lapse acquisitions, fluorescent images were captured every 30 s and phase images captured every 1 min.

For mitochondrial analysis, kymographs were produced from time-lapse stacks in ImageJ. For fast transport flux, the number of mitochondria that pass the midway point of the axon were counted in each direction. Velocities for each docked mitochondrion were measured as well as their initial distance from the growth cone. Distinguishing between fast-transported mitochondria and docked mitochondria was performed as described in detail previously (Miller and Sheetz, 2006; Roossien et al., 2013). In brief, because the velocity of fast transport driven by kinesin and dynein (360–3600 $\mu\text{m}/\text{h}$) is substantially higher than that of docked mitochondria (only \sim 25–30 $\mu\text{m}/\text{h}$ in the highest portions of the axon) these two populations are easily discernable (see kymographs in Fig. 1C,D). To be conservative, 100 $\mu\text{m}/\text{h}$ and above was used as a cut-off for excluding mitochondrial velocities from the docked population. To avoid any confounding effects of CilD converting fast-transported into docked mitochondria, any mitochondrion undergoing fast transport that halted at any time after drug addition was excluded from analysis.

Tension assay

Cultures were prepared and maintained for imaging as described above. A detailed description of the preparation and calibration of towing needles, as well as the micromanipulation of growth cones has been given previously (Lamoureux et al., 2011). In brief, micropipettes were coated with 0.01% poly-ornithine (Sigma; St Louis, MO) for 30 min, followed by a 1 mg/ml concanavalin A solution for 30 min. The growth cone was then attached to the coated needle and lifted off the substrate to allow firm attachment to the needle. After attachment, the growth cone was brought down near the dish to achieve a better plane of focus and the time-lapse imaging was begun with 20-s intervals at 40 \times magnification. A 30-min stabilizing and baseline period was observed before the addition of 100 μM ciliobrevin. CilD was prepared as described above and added to the dish manually with a long Pasteur pipette. The reference needle position was maintained unaltered through the experiment so all tension changes are attributable to the cellular response.

Acknowledgements

We thank Matthew O'Toole (Kettering University, Flint, MI) and Steve Heidemann (Michigan State University, East Lansing, MI) for helpful comments on the manuscript.

Competing interests

The authors declare no competing interests.

Author contributions

P.L. performed experiments and analyzed the data presented in Fig. 5. D.H.R. performed all other experiments and analyzed all other data. D.H.R. and K.E.M. wrote the manuscript. K.E.M. developed the model presented in Fig. 6.

Funding

This work supported by funding from the National Science Foundation [grant number IOS_0951019] to K.E.M.

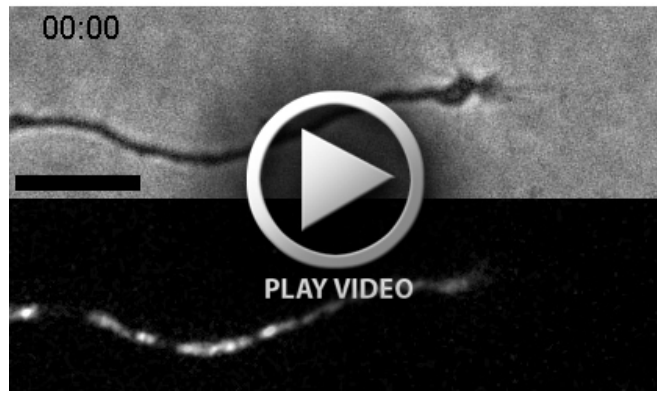
Supplementary material

Supplementary material available online at <http://jcs.biologists.org/lookup/suppl/doi:10.1242/jcs.152611/-DC1>

References

- Ahmad, F. J., Echeverri, C. J., Vallee, R. B. and Baas, P. W. (1998). Cytoplasmic dynein and dynactin are required for the transport of microtubules into the axon. *J. Cell Biol.* **140**, 391–401.
- Ahmad, F. J., Hughey, J., Wittmann, T., Hyman, A., Greaser, M. and Baas, P. W. (2000). Motor proteins regulate force interactions between microtubules and microfilaments in the axon. *Nat. Cell Biol.* **2**, 276–280.
- Ahmad, F. J., He, Y., Myers, K. A., Hasaka, T. P., Francis, F., Black, M. M. and Baas, P. W. (2006). Effects of dynactin disruption and dynein depletion on axonal microtubules. *Traffic* **7**, 524–537.
- Baas, P. W. and Ahmad, F. J. (2001). Force generation by cytoskeletal motor proteins as a regulator of axonal elongation and retraction. *Trends Cell Biol.* **11**, 244–249.
- Bell, B. J., Nauman, E. and Voytik-Harbin, S. L. (2012). Multiscale strain analysis of tissue equivalents using a custom-designed biaxial testing device. *Biophys. J.* **102**, 1303–1312.
- Bernal, R., Pullarkat, P. A. and Melo, F. (2007). Mechanical properties of axons. *Phys. Rev. Lett.* **99**, 018301.
- Carminati, J. L. and Stearns, T. (1997). Microtubules orient the mitotic spindle in yeast through dynein-dependent interactions with the cell cortex. *J. Cell Biol.* **138**, 629–641.
- Chada, S. R. and Hollenbeck, P. J. (2004). Nerve growth factor signaling regulates motility and docking of axonal mitochondria. *Curr. Biol.* **14**, 1272–1276.
- Chang, S., Rodionov, V. I., Borisy, G. G. and Popov, S. V. (1998). Transport and turnover of microtubules in frog neurons depend on the pattern of axonal growth. *J. Neurosci.* **18**, 821–829.
- Cheeseman, I. M. and Desai, A. (2008). Molecular architecture of the kinetochore-microtubule interface. *Nat. Rev. Mol. Cell Biol.* **9**, 33–46.
- Dehmelt, L., Nalbant, P., Steffen, W. and Halpain, S. (2006). A microtubule-based, dynein-dependent force induces local cell protrusions: Implications for neurite initiation. *Brain Cell Biol.* **35**, 39–56.
- del Alamo, J. C., Norwich, G. N., Li, Y. S., Lasheras, J. C. and Chien, S. (2008). Anisotropic rheology and directional mechanotransduction in vascular endothelial cells. *Proc. Natl. Acad. Sci. USA* **105**, 15411–15416.
- Dent, E. W. and Gertler, F. B. (2003). Cytoskeletal dynamics and transport in growth cone motility and axon guidance. *Neuron* **40**, 209–227.
- Dickson, B. J. (2002). Molecular mechanisms of axon guidance. *Science* **298**, 1959–1964.
- Dujardin, D. L., Barnhart, L. E., Stehman, S. A., Gomes, E. R., Gundersen, G. G. and Vallee, R. B. (2003). A role for cytoplasmic dynein and LIS1 in directed cell movement. *J. Cell Biol.* **163**, 1205–1211.
- Edelstein, A., Amodaj, N., Hoover, K., Vale, R. and Stuurman, N. (2010). Computer control of microscopes using microManager. *Curr. Protoc. Mol. Biol.* Chapter 14, Unit14.20.
- Faulkner, N. E., Dujardin, D. L., Tai, C. Y., Vaughan, K. T., O'Connell, C. B., Wang, Y. and Vallee, R. B. (2000). A role for the lissencephaly gene LIS1 in mitosis and cytoplasmic dynein function. *Nat. Cell Biol.* **2**, 784–791.
- Firestone, A. J., Weinger, J. S., Maldonado, M., Barlan, K., Langston, L. D., O'Donnell, M., Gelfand, V. I., Kapoor, T. M. and Chen, J. K. (2012). Small-molecule inhibitors of the AAA+ ATPase motor cytoplasmic dynein. *Nature* **484**, 125–129.
- Fukata, M., Watanabe, T., Noritake, J., Nakagawa, M., Yamaga, M., Kuroda, S., Matsuura, Y., Iwamatsu, A., Perez, F. and Kaibuchi, K. (2002). Rac1 and Cdc42 capture microtubules through IQGAP1 and CLIP-170. *Cell* **109**, 873–885.
- Gallo, G. (2004). Myosin II activity is required for severing-induced axon retraction in vitro. *Exp. Neurol.* **189**, 112–121.
- Gilchrist, C. L., Witvoet-Braam, S. W., Guilak, F. and Setton, L. A. (2007). Measurement of intracellular strain on deformable substrates with texture correlation. *J. Biomech.* **40**, 786–794.
- Goldberg, D. J. and Burmeister, D. W. (1986). Stages in axon formation: observations of growth of Aplysia axons in culture using video-enhanced contrast-differential interference contrast microscopy. *J. Cell Biol.* **103**, 1921–1931.
- Gomes, E. R., Jani, S. and Gundersen, G. G. (2005). Nuclear movement regulated by Cdc42, MRCK, myosin, and actin flow establishes MTOC polarization in migrating cells. *Cell* **121**, 451–463.
- Grabham, P. W., Seale, G. E., Benneceb, M., Goldberg, D. J. and Vallee, R. B. (2007). Cytoplasmic dynein and LIS1 are required for microtubule advance during growth cone remodeling and fast axonal outgrowth. *J. Neurosci.* **27**, 5823–5834.
- Gusnowski, E. M. and Srayko, M. (2011). Visualization of dynein-dependent microtubule gliding at the cell cortex: implications for spindle positioning. *J. Cell Biol.* **194**, 377–386.
- He, Y., Francis, F., Myers, K. A., Yu, W., Black, M. M. and Baas, P. W. (2005). Role of cytoplasmic dynein in the axonal transport of microtubules and neurofilaments. *J. Cell Biol.* **168**, 697–703.

- Heidemann, S. R., Lamoureux, P., Ngo, K., Reynolds, M. and Buxbaum, R. E. (2003). Open-dish incubator for live cell imaging with an inverted microscope. *Biotechniques* **35**, 708–714, 716.
- Hirokawa, N. (1982). Cross-linker system between neurofilaments, microtubules, and membranous organelles in frog axons revealed by the quick-freeze, deep-etching method. *J. Cell Biol.* **94**, 129–142.
- Hur, E. M., Yang, I. H., Kim, D. H. and Byun, J., Sajjilafu, Xu, W. L., Nicovich, P. R., Cheong, R., Levchenko, A., Thakor, N. et al. (2011). Engineering neuronal growth cones to promote axon regeneration over inhibitory molecules. *Proc. Natl. Acad. Sci. USA* **108**, 5057–5062.
- Joshi, H. C., Chu, D., Buxbaum, R. E. and Heidemann, S. R. (1985). Tension and compression in the cytoskeleton of PC 12 neurites. *J. Cell Biol.* **101**, 697–705.
- Kang, J. S., Tian, J. H., Pan, P. Y., Zald, P., Li, C., Deng, C. and Sheng, Z. H. (2008). Docking of axonal mitochondria by syntrophin controls their mobility and affects short-term facilitation. *Cell* **132**, 137–148.
- Kholmanskikh, S. S., Koeller, H. B., Wynshaw-Boris, A., Gomez, T., Letourneau, P. C. and Ross, M. E. (2006). Calcium-dependent interaction of Lis1 with IQGAP1 and Cdc42 promotes neuronal motility. *Nat. Neurosci.* **9**, 50–57.
- Kikkawa, M. (2013). Big steps toward understanding dynein. *J. Cell Biol.* **202**, 15–23.
- Knight, M. M., Bomzon, Z., Kimmel, E., Sharma, A. M., Lee, D. A. and Bader, D. L. (2006). Chondrocyte deformation induces mitochondrial distortion and heterogeneous intracellular strain fields. *Biomech. Model. Mechanobiol.* **5**, 180–191.
- Kozlowski, C., Srayko, M. and Nedelec, F. (2007). Cortical microtubule contacts position the spindle in *C. elegans* embryos. *Cell* **129**, 499–510.
- Lamoureux, P., Heidemann, S. R., Martzke, N. R. and Miller, K. E. (2010a). Growth and elongation within and along the axon. *Dev. Neurobiol.* **70**, 135–149.
- Lamoureux, P. L., O'Toole, M. R., Heidemann, S. R. and Miller, K. E. (2010b). Slowing of axonal regeneration is correlated with increased axonal viscosity during aging. *BMC Neurosci.* **11**, 140.
- Lamoureux, P., Heidemann, S. and Miller, K. E. (2011). Mechanical manipulation of neurons to control axonal development. *J. Vis. Exp.* (50).
- Lansbergen, G., Komarova, Y., Modesti, M., Wyman, C., Hoogenraad, C. C., Goodson, H. V., Lemaire, R. P., Drechsel, D. N., van Munster, E., Gadella, T. W., Jr et al. (2004). Conformational changes in CLIP-170 regulate its binding to microtubules and dynactin localization. *J. Cell Biol.* **166**, 1003–1014.
- Lee, A. C. and Suter, D. M. (2008). Quantitative analysis of microtubule dynamics during adhesion-mediated growth cone guidance. *Dev. Neurobiol.* **68**, 1363–1377.
- Lim, S. S., Edson, K. J., Letourneau, P. C. and Borisy, G. G. (1990). A test of microtubule translocation during neurite elongation. *J. Cell Biol.* **111**, 123–130.
- Lodish, H., Berk, A. and Zipursky, S. (2000). *Molecular Cell Biology*, 4th edn. New York, NY: W. H. Freeman.
- Lowery, L. A. and Van Vactor, D. (2009). The trip of the tip: understanding the growth cone machinery. *Nat. Rev. Mol. Cell Biol.* **10**, 332–343.
- Lu, W., Fox, P., Lakonishok, M., Davidson, M. W. and Gelfand, V. I. (2013). Initial neurite outgrowth in *Drosophila* neurons is driven by kinesin-powered microtubule sliding. *Curr. Biol.* **23**, 1018–1023.
- Markus, S. M., Punch, J. J. and Lee, W. L. (2009). Motor- and tail-dependent targeting of dynein to microtubule plus ends and the cell cortex. *Curr. Biol.* **19**, 196–205.
- Martin, M., Iyadurai, S. J., Gassman, A., Gindhart, J. G., Jr, Hays, T. S. and Saxton, W. M. (1999). Cytoplasmic dynein, the dynactin complex, and kinesin are interdependent and essential for fast axonal transport. *Mol. Biol. Cell* **10**, 3717–3728.
- Mazel, T., Biesemann, A., Krejczyk, M., Nowald, J., Muller, O. and Dehmelt, L. (2014). Direct observation of microtubule pushing by cortical dynein in living cells. *Mol. Biol. Cell.* **25**, 95–106.
- Miller, K. E. and Sheetz, M. P. (2004). Axonal mitochondrial transport and potential are correlated. *J. Cell Sci.* **117**, 2791–2804.
- Miller, K. E. and Sheetz, M. P. (2006). Direct evidence for coherent low velocity axonal transport of mitochondria. *J. Cell Biol.* **173**, 373–381.
- Morris, R. L. and Hollenbeck, P. J. (1993). The regulation of bidirectional mitochondrial transport is coordinated with axonal outgrowth. *J. Cell Sci.* **104**, 917–927.
- Myers, K. A., Tint, I., Nadar, C. V., He, Y., Black, M. M. and Baas, P. W. (2006). Antagonistic forces generated by cytoplasmic dynein and myosin-II during growth cone turning and axonal retraction. *Traffic* **7**, 1333–1351.
- O'Connell, C. B. and Wang, Y. L. (2000). Mammalian spindle orientation and position respond to changes in cell shape in a dynein-dependent fashion. *Mol. Biol. Cell* **11**, 1765–1774.
- O'Toole, M., Lamoureux, P. and Miller, K. E. (2008). A physical model of axonal elongation: force, viscosity, and adhesions govern the mode of outgrowth. *Biophys. J.* **94**, 2610–2620.
- Okabe, S. and Hirokawa, N. (1990). Turnover of fluorescently labelled tubulin and actin in the axon. *Nature* **343**, 479–482.
- Palazzo, A. F., Joseph, H. L., Chen, Y. J., Dujardin, D. L., Alberts, A. S., Pfister, K. K., Vallee, R. B. and Gundersen, G. G. (2001). Cdc42, dynein, and dynactin regulate MTOC reorientation independent of Rho-regulated microtubule stabilization. *Curr. Biol.* **11**, 1536–1541.
- Pathak, D., Sepp, K. J. and Hollenbeck, P. J. (2010). Evidence that myosin activity opposes microtubule-based axonal transport of mitochondria. *J. Neurosci.* **30**, 8984–8992.
- Pavin, N. and Tolić-Nørrelykke, I. M. (2013). Dynein, microtubule and cargo: a ménage à trois. *Biochem. Soc. Trans.* **41**, 1731–1735.
- Pilling, A. D., Horiuchi, D., Lively, C. M. and Saxton, W. M. (2006). Kinesin-1 and Dynein are the primary motors for fast transport of mitochondria in *Drosophila* motor axons. *Mol. Biol. Cell* **17**, 2057–2068.
- Reinsch, S. S., Mitchison, T. J. and Kirschner, M. (1991). Microtubule polymer assembly and transport during axonal elongation. *J. Cell Biol.* **115**, 365–379.
- Roossien, D. H., Lamoureux, P., Van Vactor, D. and Miller, K. E. (2013). *Drosophila* growth cones advance by forward translocation of the neuronal cytoskeletal meshwork in vivo. *PLoS ONE* **8**, e80136.
- Saxton, W. M. and Hollenbeck, P. J. (2012). The axonal transport of mitochondria. *J. Cell Sci.* **125**, 2095–2104.
- Schaefer, A. W., Kabir, N. and Forscher, P. (2002). Filopodia and actin arcs guide the assembly and transport of two populations of microtubules with unique dynamic parameters in neuronal growth cones. *J. Cell Biol.* **158**, 139–152.
- Schaefer, A. W., Schoonderwoert, V. T., Ji, L., Medeiros, N., Danuser, G. and Forscher, P. (2008). Coordination of actin filament and microtubule dynamics during neurite outgrowth. *Dev. Cell* **15**, 146–162.
- Schnapp, B. J. and Reese, T. S. (1989). Dynein is the motor for retrograde axonal transport of organelles. *Proc. Natl. Acad. Sci. USA* **86**, 1548–1552.
- Silberberg, Y. R. and Pelling, A. E. (2013). Quantification of intracellular mitochondrial displacements in response to nanomechanical forces. *Methods Mol. Biol.* **991**, 185–193.
- Stuessi, M. and Bradke, F. (2011). Neuronal polarization: the cytoskeleton leads the way. *Dev. Neurobiol.* **71**, 430–444.
- Straight, A. F., Cheung, A., Limouze, J., Chen, I., Westwood, N. J., Sellers, J. R. and Mitchison, T. J. (2003). Dissecting temporal and spatial control of cytokinesis with a myosin II inhibitor. *Science* **299**, 1743–1747.
- Suter, D. M. and Miller, K. E. (2011). The emerging role of forces in axonal elongation. *Prog. Neurobiol.* **94**, 91–101.
- Vale, R. D. (2003). The molecular motor toolbox for intracellular transport. *Cell* **112**, 467–480.
- Vallee, R. B., Seale, G. E. and Tsai, J. W. (2009). Emerging roles for myosin II and cytoplasmic dynein in migrating neurons and growth cones. *Trends Cell Biol.* **19**, 347–355.
- Vaughan, K. T., Tynan, S. H., Faulkner, N. E., Echeverri, C. J. and Vallee, R. B. (1999). Colocalization of cytoplasmic dynein with dynactin and CLIP-170 at microtubule distal ends. *J. Cell Sci.* **112**, 1437–1447.
- Wagner, O. I., Lifshitz, J., Janmey, P. A., Linden, M., McIntosh, T. K. and Leterrier, J. F. (2003). Mechanisms of mitochondria-neurofilament interactions. *J. Neurosci.* **23**, 9046–9058.
- Wang, N., Naruse, K., Stamenović, D., Fredberg, J. J., Mijailovich, S. M., Tolić-Nørrelykke, I. M., Polte, T., Mannix, R. and Ingber, D. E. (2001). Mechanical behavior in living cells consistent with the tensegrity model. *Proc. Natl. Acad. Sci. USA* **98**, 7765–7770.
- Wang, N., Hu, S. and Butler, J. P. (2007). Imaging stress propagation in the cytoplasm of a living cell. *Methods Cell Biol.* **83**, 179–198.
- Watanabe, T., Wang, S., Noritake, J., Sato, K., Fukata, M., Takefuji, M., Nakagawa, M., Izumi, N., Akiyama, T. and Kaibuchi, K. (2004). Interaction with IQGAP1 links APC to Rac1, Cdc42, and actin filaments during cell polarization and migration. *Dev. Cell* **7**, 871–883.
- Yi, J. Y., Ori-McKenney, K. M., McKenney, R. J., Vershinin, M., Gross, S. P. and Vallee, R. B. (2011). High-resolution imaging reveals indirect coordination of opposite motors and a role for LIS1 in high-load axonal transport. *J. Cell Biol.* **195**, 193–201.



Movie 1. Disruption of dynein with Ciliobrevin D slows axonal elongation and induces retraction of the axonal cytoskeleton. Elongating axons treated with 100 μ M CilD (t=18:00 min) display brief axonal retraction followed by a stationary phase as seen in the phase panel. The mitochondria in the growth cone and distal axon retract even after the growth cone pauses. Scale bar=20 μ m. Movie plays at 7 frames per second.



Movie 2. Focal disruption of dynein in growth cone and distal axon causes axonal retraction. CilD (left column) and DMSO (right column) were mixed with TexasRed-dextran and focally applied to the growth cone and distal region of the axons. The fluid is shown as shown as red fluorescent overlay in the top row. Growth cones treated with CilD undergo retraction while those treated with DMSO continue to advance. Scale bar=20 μ m. Movie plays at 7 frames per second.



Movie 3. Dynein disruption increases axonal tension. Tension is measured by measuring the distance in deflection between a calibrated micropipette attached to a growth cone (left needle) and a stationary reference needle (right needle). After a steady-state rest tension is reached, 100 μ M Ciliobrevin D is added (t=30:00 min) and tension in the axon increases as evidenced by the increased pulling on the calibrated needle. Scale bar=20 μ m. Movie plays at 30 frames per second.